Amino Acids (2010) 39:739–750
DOI 10.1007/s00726-010-0513-7

ORIGINAL ARTICLE

The interaction of zinc with membrane-associated 18.5 kDa myelin basic protein: an attenuated total reflectance-Fourier transform infrared spectroscopic study

Graham S. T. Smith · Lin Chen · Vladimir V. Bamm · John R. Dutcher · George Harauz

Received: 23 November 2009 / Accepted: 3 February 2010 / Published online: 19 February 2010

Abstract Myelin basic protein (MBP) is an essential structural protein required for tight compaction of the myelin sheath of the central nervous system, and belongs to the family of intrinsically disordered proteins. It contains a high proportion of polar and charged amino acids, and has an adaptive conformation depending on its environment and binding surfaces (membranes) or partners (other proteins or small ligands including divalent cations). Zinc is an important stabilizing component of myelin and its concentration is substantially higher than that of any other trace element in the brain. In this study, we investigate the effect of zinc on different variants of 18.5 kDa MBP, including new recombinant forms lacking hexahistidine tags which would interfere with the binding of the cation. Isothermal titration calorimetry showed the dissociation constant to be in the micromolar range for all variants. Circular dichroism spectroscopy showed that there was minimal effect of zinc on the secondary structure on MBP in aqueous solution. When MBP was reconstituted with myelin-mimetic membranes, attenuated total reflectance-Fourier transform infrared spectroscopy revealed that there was a rearrangement of secondary structure components upon addition of zinc that was subtly different for each variant, indicative of a synergistic protein–membrane–cation interaction.

Keywords Myelin basic protein (MBP) · Intrinsically disordered protein · Induced folding · Isothermal titration calorimetry (ITC) · Circular dichroism (CD) · Fourier transform infrared (FTIR) spectroscopy · Attenuated total reflectance (ATR) spectroscopy

Abbreviations

ATR	Attenuated total reflectance
CD	Circular dichroism
CNS	Central nervous system
Cyt-LUV	Large unilamellar vesicle with lipid composition, of inner oligodendrocyte membrane leaflet
ddH_2O	Double-distilled water
EDTA	Ethylenediamine tetraacetic acid
FTIR	Fourier transform infrared
HEPES	*N*-(2-Hydroxyethyl) piperazine-*N*′-2-ethanesulfonic acid
HPLC	High-performance liquid chromatography
IDP	Intrinsically disordered protein
IEX	Ion-exchange (chromatography)
IPTG	Isopropyl-β-D-thiogalactopyranoside
ITC	Isothermal titration calorimetry
MBP	Myelin basic protein
OD	Optical density
PAGE	Polyacrylamide gel electrophoresis
PCR	Polymerase chain reaction
rmC1	Recombinant murine 18.5 kDa MBP, unmodified (LEH_6-tagged)

G. S. T. Smith, L. Chen and V. V. Bamm contributed equally to this work.

G. S. T. Smith · L. Chen · V. V. Bamm · G. Harauz (✉)
Department of Molecular and Cellular Biology,
University of Guelph, 50 Stone Road East,
Guelph, ON N1G 2W1, Canada
e-mail: gharauz@uoguelph.ca

L. Chen · J. R. Dutcher
Department of Physics, University of Guelph,
Guelph, ON N1G 2W1, Canada

rmC8	Recombinant murine 18.5 kDa MBP, pseudo-deiminated (LEH_6-tagged)
SDS	Sodium dodecyl sulphate
UT-rmC1	Untagged recombinant murine 18.5 kDa MBP, unmodified
UT-rmC8	Untagged recombinant murine 18.5 kDa MBP, pseudo-deiminated

Introduction

Myelin basic protein (MBP), particularly the 18.5 kDa isoform, is essential for maintaining the stability of the myelin sheath of the central nervous system (CNS) (Boggs 2006, 2008; Harauz et al. 2009). Ablation of or mutations in the MBP gene result in the loss of compact myelin in the CNS, e.g., *shiverer* (*shi*) mice (Readhead and Hood 1990) or the Long Evans *shaker* (*les*) rat (Carré et al. 2002). Myelin basic protein can be classified as an intrinsically disordered protein (IDP) (Uversky 2009) because it has a considerable proportion of predicted disorder (Libich and Harauz 2008a; Harauz and Libich 2009; cf., Bailey et al. 2001). This intrinsic flexibility facilitates interaction with a diverse variety of surfaces, other proteins, or small ligands, indicative of a complex structure–function relationship as recently reviewed (Harauz et al. 2004, 2009; Harauz and Libich 2009). In all associations that have so far been investigated structurally (phospholipid membrane, Ca^{2+}-calmodulin, actin), the 18.5 kDa MBP isoform has demonstrated a partial induced disorder-to-order transition, including several α-helical molecular recognition fragments (Libich and Harauz 2008a; Harauz and Libich 2009; Libich et al. 2010). All complexes can be described as "fuzzy" since much of the protein remains highly mobile within them, meaning that there is no rigid tertiary structure in the usual sense in which it is conceived (Libich et al. 2010; Tompa and Fuxreiter 2008; Mittag et al. 2009). The conformational polymorphism of MBP is consistent with its in vivo roles as a scaffold, linker, and signaling hub for, e.g., membranes, cytoskeleton, Ca^{2+}-calmodulin, SH3-proteins (Harauz et al. 2009).

Another stabilizing component of CNS myelin is zinc, with a concentration (about 50 μM) that is substantially higher than that of any other trace element (Iyengar et al. 1978; Koh 2001). Zinc deficiency leads to abnormal CNS development and neuropsychological impairment (Keen et al. 1993; Sandstead et al. 2000; Koh 2001; Takeda 2001; Unal et al. 2005). Abnormally high levels of zinc have been reported in neurofibrillary tangles associated with various neurodegenerative diseases (e.g., reviewed in Mo et al. 2009). Using X-ray diffraction, Inouye and Kirschner (1984) showed that zinc caused peripheral nervous system myelin to retain sharp reflections (i.e., a compact structure), and it is conceivable that the same result would be obtained with CNS myelin in which MBP predominates. Almost all of the zinc in brain white matter is protein-bound (Itoh et al. 1983), and MBP has been identified specifically as a zinc-binding protein via its histidyl residues (Berlet et al. 1994; Tsang et al. 1997) with a reported dissociation constant of 0.44 μM (Saeidian et al. 2001). When the MBP is solubilized in phosphate buffer, the addition of zinc results in large aggregates (Cavatorta et al. 1994; Riccio et al. 1995), and the cation is thus believed to stabilize the protein's association to myelin membranes (Earl et al. 1988; Berlet et al. 1991). It has been shown by X-ray absorption spectroscopy of reconstituted Langmuir–Blodgett multilayers that Zn^{2+} ions bind to both MBP and phospholipid headgroups (Morante 2001; Nuzzo et al. 2002; Benfatto et al. 2004). In multiple sclerosis patients, zinc levels in erythrocytes have been observed to increase dramatically ($\sim 3\times$), perhaps due to disruption of normal compartmentalization of zinc during demyelination (Ho et al. 1986).

In this study, we test specifically the hypothesis that zinc induces ordered secondary structure in 18.5 kDa MBP, as it does for several other IDPs (Gatewood et al. 1990; Uversky et al. 2000; Uversky 2009). The previous studies cited above have used MBP preparations obtained from brain myelin, which are heterogeneous mixtures of charged components comprising myriad post-translational modifications (Kim et al. 2003; Harauz et al. 2004). Our group has introduced the use of recombinant murine MBP isoforms that yield very pure (compositionally homogeneous) protein samples for biochemical and structural studies. Our two main prototypes are unmodified 18.5 kDa murine MBP (generically rmMBP, specifically rmC1) (Bates et al. 2000), which emulates the predominant, minimally modified C1 component of healthy myelin, and rmC8 with six R/K-to-Q substitutions to mimic citrullination in the highly modified C8 component, which is found in increased proportion in multiple sclerosis (Bates et al. 2002). The net charges at neutral pH are +19 and +13 for rmC1 and rmC8, respectively. In previous solution NMR spectroscopic experiments on rmC1, we have shown that there was negligible effect of Ca^{2+} on the ^{1}H–^{15}N heteronuclear single quantum coherence spectra of the protein, but that Zn^{2+} perturbed the spectra subtly (Libich and Harauz 2008b). We concluded that future studies of the interactions of Zn^{2+} with rmMBP required the construction of variants lacking the hexahistidine tag (which would interact with any cation).

In this current work, we describe new protein constructs lacking this His_6-tag (UT-rmC1 and UT-rmC8, respectively) and the optimization of their purification. Using circular dichroic (CD) spectroscopy, we show that there is

minimal effect of zinc on the secondary structure of either UT-rmC1 or UT-rmC8 in aqueous solution. However, when these proteins were reconstituted with myelin-mimetic membranes, attenuated total reflectance-Fourier transform infrared (ATR-FTIR) spectroscopy demonstrated a subtle conformational shift, primarily a slight increase in α-helicity, in both of these new protein variants.

Materials and methods

Construction of UT-rmMBP expression plasmids

The previously described pET22b-rmC1 and pET22b-rmC8 plasmids containing the complete open reading frame for murine 18.5 kDa MBP were used as templates to construct the un-tagged pET22b-UT-rmC1 and pET22b-UT-rmC8 protein expression plasmids, respectively. These constructs were created by introducing a stop codon between the hexahistidine tag and the open reading frame for mMBP using Quikchange site-directed mutagenesis (Stratagene, La Jolla, CA, USA). For all polymerase chain reactions (PCR), synthetic oligonucleotides were purchased from Sigma-Aldrich (Oakville, ON, USA). The forward and reverse primers (FP and RP, respectively) used to produce pET22b-rmC1 and pET22b-rmC8 were:

Stop *XhoI* *6x His* →

rmC1-FP: 5′ CCATGGCGAGACGC**TGA**CTCGAG**CACCACCACC** 3′

rmC1-RP: 5′ GGTGGTGGTGCTCGAGTCAGCGTCTCGCCATGG 3′

Stop *XhoI* *6x His* →

rmC8-FP: 5′ CCATGGCGAGACAA**TGA**CTCGAG**CACCACCACC** 3′

rmC8-RP: 5′ GGTGGTGGTGCTCGAGTCATTGTCTCGCCATGG 3′

Each 50 μL mutagenesis reaction consisted of 1 μL of 250 ng stock of plasmid (template) DNA, 1 μL of a 150 mM stock of mutagenic forward and reverse primer, 5 μL of 10× *Pfu* Ultra Buffer, 41.5 μL ddH_20, and 0.5 μL of *Pfu* Ultra DNA polymerase (2.5 units μL^{-1}). The PCR site-directed mutagenesis was performed using a BioRad thermal cycler PCR system with the following cycling parameters: initial denaturing temperature of 95°C for 30 s, followed by 18 cycles of 95°C (denaturing temperature) for 30 s, 55°C (annealing temperature) for 1 min, 68°C (extension temperature) for 12 min followed by a final extension at 68°C for 10 min, with the completed reaction being held at 4°C. Any remaining non-mutated parental DNA was eliminated by adding 0.5 μL of *Dpn*I (10 units μL^{-1}) restriction enzyme directly to the PCR reaction. The restriction digest was incubated at 37°C for 4 h, and 5 μL was subsequently transformed into *E. coli* DH5α and plated on Luria–Bertani plates containing 50 μg mL^{-1} of ampicillin. A single colony obtained from each transformation reaction was grown in Luria–Bertani media. The plasmid DNA was extracted using Roche High Pure Plasmid isolation kit (Roche Diagnostics, IN, USA) and was confirmed by sequencing (Laboratory Services Division, University of Guelph).

Protein over-expression and purification

Plasmids that were confirmed by sequencing to encode the UT-rmC1 and UT-rmC8 proteins were transformed into *E. coli* BL-21-CodonPlus (DE3)pLysS cells (Stratagene) and were expressed and purified as described below. A 150 mL Luria–Bertani culture containing 50 μg mL^{-1} ampicillin and 34 μg mL^{-1} chloramphenicol was inoculated using an overnight culture of *E. coli* transformed with either the pET22b-UT-rmC1 or pET22b-UT-rmC8 plasmid, and grown at 37°C to an optical density (600 nm) of 0.6–0.8. This culture was centrifuged at 4,000×*g* for 15 min at room temperature and was transferred to a 1 L culture of pre-warmed M9 minimal media containing the same concentrations of antibiotic mentioned above. Again, cultures were grown to an optical density (OD at 600 nm) of 0.6 and were induced for 6 h with 1 mM IPTG (isopropyl-*β*-D-thiogalactopyranoside).

The cell pellet was resuspended in 100 mL of lysis buffer containing 8 M urea, 100 mM NaH_2PO_4, 10 mM Tris-base, 500 mM NaCl and 1% Tween-20 (v/v), pH 9.5. The mixture was stirred at room temperature for about 40 min, and then freeze-thawed twice. Afterwards, the lysate was centrifuged at 25,000×*g* for 45 min; the supernatant was collected and dialyzed against ion-exchange chromatography buffer (IEX buffer) consisted of 6 M urea, 80 mM glycine, pH 9.5 (three changes). Next, the dialysate was filtered through a 0.8/0.2 μm membrane filter and was loaded onto a 5 mL CM-HighTrap FF column (GE Heathcare Bio-sciences Inc.) that was previously charged using 50 mL of 1 M NaCl in IEX buffer, following equilibration using 50 mL of IEX buffer. The column was washed with IEX buffer until the absorbance reading at 280 nm was under 0.01. The protein was eluted using 50 mL of 0–0.2 M NaCl linear gradient in IEX buffer at a flow rate of 1 mL min^{-1}. All fractions were analyzed using SDS-PAGE and absorbance was measured at 280 nm to determine purity and concentration, respectively (*vide infra*). Pure protein fractions were pooled and dialyzed slowly in a sequential fashion to remove salts and denaturing agents, using tubing with a M_r cutoff of 6,000–8,000 Da. Dialysis buffers were as follows: (a) 50 mM Tris–HCl, pH 7.4, 250 mM NaCl (two changes); (b) 100 mM NaCl (two changes); (c) double-distilled water

(four changes). After the final dialysis step, the protein was frozen and finally lyophilized.

Two other proteins containing the hexahistidine tag, rmC1 and rmC8, were purified using our standard protocols (Bates et al. 2000, 2002; Hill et al. 2003). Throughout these investigations, protein concentrations were quantified by measuring the absorbance at 280 nm. The protein extinction coefficients used were 0.667 L g^{-1} cm^{-1} for rmC1, 0.672 L g^{-1} cm^{-1} for rmC8, 0.705 L g^{-1} cm^{-1} for UT-rmC1, and 0.711 L g^{-1} cm^{-1} for UT-rmC8 (as calculated by SwissProt for protein in 6.0 M guanidine hydrochloride, 0.02 M phosphate, pH 6.5). The accuracy of this approach had previously been verified by amino acid analysis (Bates et al. 2000, 2002). Protein preparations were routinely analyzed using sodium dodecyl sulphate-polyacrylamide gel electrophoresis (SDS-PAGE) and staining with Coomassie Brilliant Blue R250 (Fisher Scientific, Unionville, ON, USA).

Reversed-phase HPLC

Reversed-phase high performance liquid chromatography (HPLC) was employed to assess the final purity of UT-rmC1 and UT-rmC8 proteins following the purification procedure, using a previously published protocol with small modifications (Bamm and Harauz 2008). The HPLC system comprised a Waters 626 Gradient Pump, a Waters 2487 Variable Wavelength Dual Channel UV Detector, 50 µL sample loop, and a Waters Symmetry 300™ C18 column (5 µm, 4.6 × 150 mm^2). Detection was at 214 nm, the flow rate was 1 mL min^{-1} and 0.5 mL min^{-1} for UT-rmC1 and UT-rmC8, respectively, and the column was maintained at 25°C. Acetonitrile (ACN) and trifluoroacetic acid (TFA) were used as the mobile phase and ion-pairing agent, respectively. After 2 min of loading time at 10% acetonitrile and 0.1% TFA, the elution gradients started from 10 to 50% acetonitrile, and 0.1% trifluoroacetic acid, at a rate of 1% acetonitrile per min, followed by 5% per min for an additional 10 min.

Isothermal titration calorimetry

Isothermal titration calorimetry (ITC) experiments were carried out using a VP-ITC instrument from Microcal Inc. (Northampton, MA, USA). Lyophilized variants of rmMBP were dissolved in buffer (20 mM HEPES–NaOH, pH 7.4, 100 mM NaCl), and extensively dialyzed against the same solution (at least 4 changes). Following the dialysis, the protein was filtered (0.22 µm pore size) and the concentration was measured from the absorbance at 280 nm. The stock of 2.5 mM $ZnCl_2$ was prepared in the same solution prior to each experiment. Samples were degassed in a Thermovac (Northhampton, MA, USA) at 25°C for 10 min. The Zn^{2+} solution (2.5 mM) was injected into the sample cell, containing 50 µM of rmMBP variant in the above solution. Typically, the titrations were carried out with a preliminary injection of 2 µL followed by 24 injections of 5 µL of ligand solution, and then 17 injections of 7 µL of ligand solution, with a 300 s spacing between each injection. All experiments were carried out in triplicate at 25°C. Before analysis, data from the preliminary 2 µL injection were discarded, and heats of dilution of the ligand (Zn^{2+}) into solution of 20 mM HEPES–NaOH, pH 7.4, 100 mM NaCl (in the absence of rmMBP variants) were subtracted from the ligand (Zn^{2+}) into rmMBP experiments. The corrected data were integrated and plotted as a function of the molar ratio, and the binding isotherms obtained were fitted to the Origin "one set of sites" and/or "two sets of sites" models (Origin 5.0, Microcal) (cf., Majava et al. 2008).

Circular dichroism spectroscopy

Circular dichroism (CD) was performed using a Jasco J-815 spectropolarimeter (Japan Spectroscopic Co., Tokyo, Japan) using an initial protein concentration of 1.3 mg mL^{-1} in a sample volume of 70 µL in a quartz cuvette with a path length of 0.1 mm. The far-UV CD spectra (190–250 nm) were scanned at a rate of 50 nm min^{-1}, with data collection at 1 nm intervals, at 25°C. The blank was subtracted after each measurement, and the spectra from six successive scans were averaged for each sample. The molar ellipticities were calculated using the protein concentrations and molar mass. The CD measurements were carried out for each protein variant in two different aqueous solutions: (1) 20 mM HEPES–NaOH, pH 7.4, 100 mM NaCl; and (2) 20 mM HEPES–NaOH, pH 7.4, 100 mM NaCl, 1.3 mM $ZnCl_2$.

Sample preparation for ATR-FTIR spectroscopy

Protein samples were dissolved in a HEPES buffer (20 mM HEPES–NaOH, pH 7.4, 100 mM NaCl) at a concentration of approximately 4 mg mL^{-1}, determined by absorbance at 280 nm. Protein solutions were stored at −20 °C to prevent degradation. The $ZnCl_2$ was dissolved in the same HEPES buffer at a concentration of 10 mM and stored at room temperature.

Large unilamellar vesicles (LUVs) with lipid composition similar to that of the cytoplasmic monolayer of myelin (Cyt-LUVs; cholesterol:phosphatidylethanolamine:phosphatidylserine:phosphatidylcholine:sphingomyelin:phosphatidylinositol in 44:27:13:11:3:2 M ratios) (Inouye and Kirschner 1988) were prepared by extrusion as previously described (Boggs et al. 1997; Musse et al. 2006; Zhong et al. 2007). Lipids were purchased from Avanti Polar Lipids (Alabaster,

AL, USA). Various lipid stocks in chloroform mixtures (chloroform:H_2O:methanol 1:2:1, vol), were mixed to the desired molar ratio. Chloroform was then evaporated under a mild nitrogen flow and subsequently kept under vacuum overnight for complete removal of the chloroform remnants. Lipid mixtures were rehydrated in the same HEPES buffer at 45°C overnight with vigorous shaking and three freeze–thaw cycles. Large unilamellar vesicles (LUVs) were formed by extruding the lipid mixture 61 times through a polycarbonate membrane with a 100 nm pore size, at 45°C. The sizes of vesicles were confirmed to be around 100 nm using a Zetasizer Nano-S model ZEN1600 (633 nm "red" laser; Malvern Instruments) Dynamic Light Scattering (DLS) instrument. The final concentration was determined by a modified Micro-Bartlett Phosphorus Assay (Bartlett 1959).

Protein solutions were diluted with the above HEPES buffer to a concentration that matched the lipid vesicles before mixing (around 4 mg mL^{-1}). In the experiments studying the effect of Zn^{2+}, concentrated Zn^{2+}-containing HEPES buffer was added to the protein solution first (to reach the final Zn^{2+} concentration of 20 times molarity as that of protein), followed by a 5 min incubation at room temperature and subsequent addition of the Cyt-LUV solution to reach a 1:1 (mass:mass) protein–lipid ratio. This relatively high protein–lipid ratio was necessary to obtain an adequate signal-to-noise ratio in the ATR-FTIR experiments. (We do not believe that there is significant protein–protein interaction under these conditions, because ^{13}C spectra recorded for different protein:lipid mass ratios up to 0.7 were essentially identical as ascertained by solid-state NMR spectroscopy (Zhong et al. 2007). A subsequent incubation of 10-15 min allowed a further equilibration of the protein–lipid interaction.

ATR-FTIR spectroscopy and data analysis

The spectra were recorded using a BrukerOptics Vertex70 FTIR spectrometer equipped with a liquid nitrogen-cooled mercury cadmium telluride (MCT) detector. A vertical PIKE MIRacle Micro ATR accessory (PIKE technologies, USA), combined with a three-reflection diamond crystal unit (diameter 6 mm), was used. The diamond three-reflection ATR crystal was cleaned by double-distilled H_2O, followed by isopropanol to eliminate trace water. For each spectrum, 200 interferograms were collected and Fourier-transformed to give a resolution of 2 cm^{-1}. During measurement, the optics compartment and the sample compartment of the spectrometer were purged continuously with dry nitrogen gas to eliminate spectral contributions from atmospheric water vapor. All experiments were conducted at room temperature ($\sim$22°C).

After incubation, the protein-LUV complex (with or without Zn^{2+}) was spun down in a table-top centrifuge at 14,000 rpm (18,000×g) for 1 h. The supernatant was then removed. Aggregates were carefully spread onto the surface of the three-reflection diamond ATR crystal. A stream of nitrogen gas, containing rich D_2O vapor, flowed over the crystal until the sample was completely deuterated. Upon $^1H/^2H$ exchange, the absorption band associated with the random secondary structure shifts from about 1,655 cm^{-1} to about 1,642 cm^{-1}. This change permits differentiation of the α-helical and the random secondary structures (Susi et al. 1967; Byler and Susi 1986). Spectra in the range from 950 to 1,750 cm^{-1} were collected. A typical measurement required approximately 200 μg of each variant of rmMBP.

The overlapping bands were resolved by Fourier self-deconvolution using OMNIC software (Thermo Fisher Scientific, Waltham, MA, USA). The bandwidth value was set to 15 and the enhancement value was set to 1.8. The frequencies of these component bands were subsequently used in PeakFit software (Seasolve Software Inc., San Jose, CA, USA; version 4.12) as input parameters for curve-fitting analysis of the original spectrum. The amide I region ($\sim$1,620 to $\sim$1,700 cm^{-1}) involves the peptide backbone C=O stretch and N–H groups, and bond angles were analyzed for protein secondary structure composition. The spectra of the rmMBP variants in Cyt-LUVs were deconvolved using a mixed Gaussian and Lorentzian band shape of standard deviation 8.5. Auto-fits of the second derivative of the original spectra were performed until the coefficient of determination (r^2) was larger than 0.99. The integrated areas derived from the curve-fitting analyses were used in calculating the various conformational states assigned to individual bands.

Results and discussion

Purification and yield of UT-rmC1 and UT-rmC8

Previously we have described procedures to purify and extract His_6-tagged versions of rmC1 and rmC8 using nickel affinity followed by ion-exchange chromatography to achieve an overall purity of $\sim$95% (Bates et al. 2000, 2002). Subsequent optimization resulted in yields of at least 10 mg isotopically labeled rmMBP per liter of M9 minimal media for NMR spectroscopy (Libich et al. 2004). In this study, we have described a new purification protocol that isolates un-tagged (UT) versions of these recombinant proteins using a denaturing lysis procedure followed by ion-exchange chromatography. The denaturing lysis procedure was introduced to extract rmMBP from the inclusion bodies to produce a sample suitable for ion-exchange chromatography (Fig. 1). A one-step purification protocol employing ion-exchange chromatography allowed for isolation of UT-rmC1 and UT-rmC8 with purity greater than

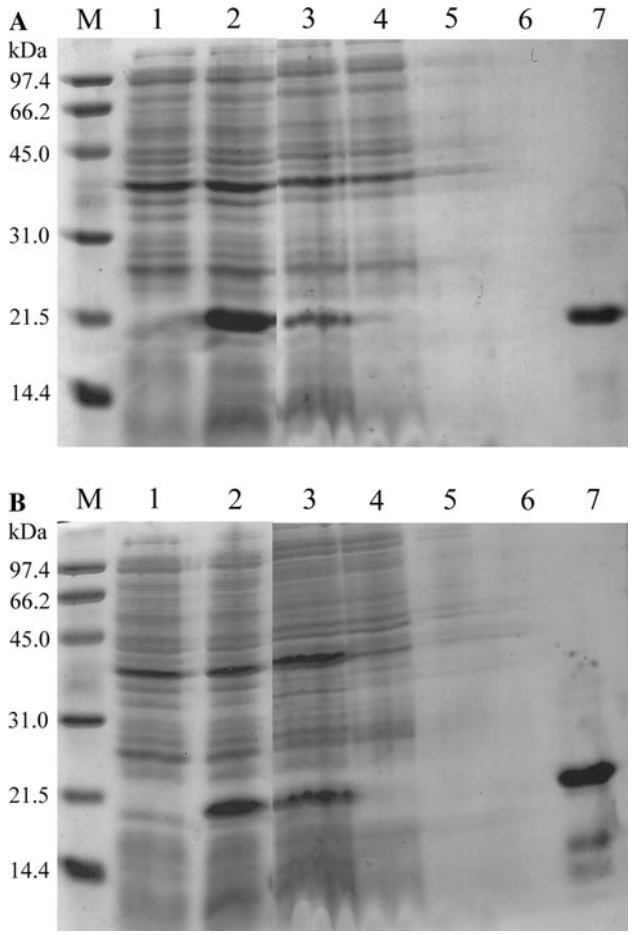

Fig. 1 Purification of **a** UT-rmC1 and **b** UT-rmC8 from *E. coli* BL-21-CodonPlus (DE3)pLysS using a denaturing lysis procedure followed by ion-exchange chromatography. Each SDS-polyacrylamide gel shows the stages throughout purification: *M* molecular mass markers; *Lane 1*, pre-induction of *E. coli* culture; *Lane 2*, 6 h post-induction sample from *E. coli* culture after induction with 1 M isopropyl-*β*-D-thiogalactopyranoside (IPTG); *Lane 3*, crude protein sample from the lysate conditioned for ion-exchange chromatography; *Lane 4*, flow-through of ion-exchange chromatography; *Lane 5*, first column wash with IEX buffer (from the first 50 mL); *Lane 6*, second column wash with IEX buffer (from the next 20 mL); *Lane 7*, pooled fractions of the eluted purified protein before dialysis

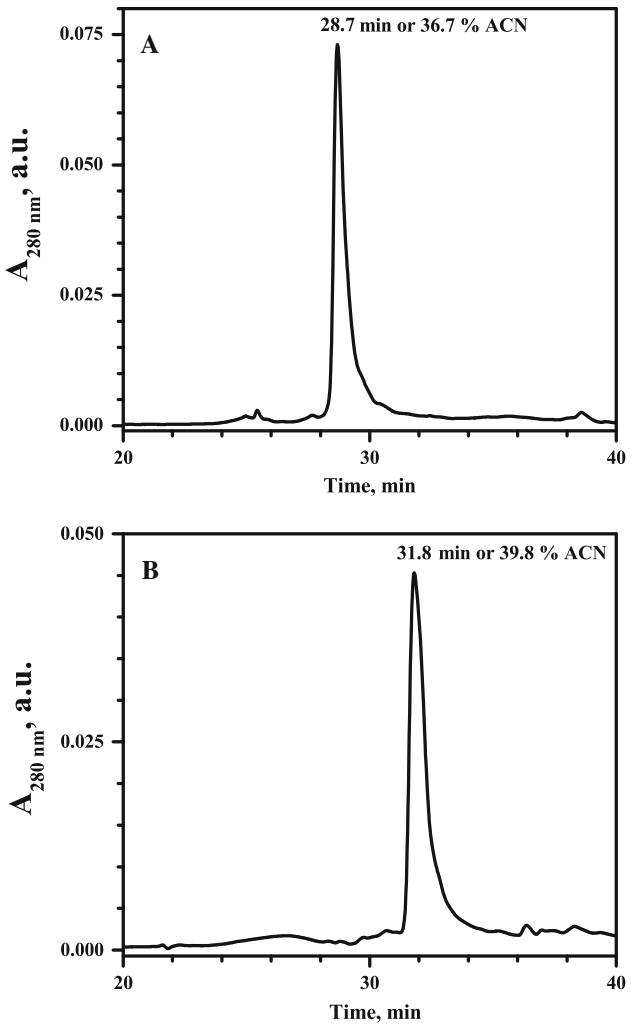

Fig. 2 The HPLC profiles of **a** UT-rmC1 and **b** UT-rmC8 final dialyzed product of pooled purified fractions from ion-exchange chromatography. For UT-rmC1 the flow rate was 1 mL min^{-1} with a gradient of 1% acetonitrile min^{-1}, whereas for UT-rmC8 the flow rate was 0.5 mL min^{-1} with a gradient of 1% acetonotrile min^{-1}. The total gradient in all cases was from 10% acetonitrile in water with 0.1% trifluoroacetic acid, to 100% acetonitrile with 0.1% trifluoroacetic acid. The purity was calculated from the chromatograms by assessing the integrated area of the major peak of each profile, and was 97% for UT-rmC1, and 96.4% for UT-rmC8

96%. Using HPLC, the UT-rmC1 and UT-rmC8 preparations were determined to have a purity of 97 and 96.4%, respectively, by assessing the integrated peak areas of each individual profile (Fig. 2). A typical yield from 1 L of M9 medium for UT-rmC1 and UT-rmC8 was 8 and 6 mg, whereas the maximal amount of protein isolated from the purification procedure was 17 and 12 mg, respectively. We were thus able to optimize the purification procedure for UT-rmC1 and UT-rmC8 to have equal purity and nearly equal protein yield as for our hexahistidine-tagged versions.

Binding of Zn^{2+} assessed by isothermal titration calorimetry

Previous studies have indicated that MBP binds divalent cations, particularly Zn^{2+} and Cu^{2+} (Berlet et al. 1994). These interactions were shown to inhibit dissociation of MBP from the membrane (Earl et al. 1988). Thus, we decided to probe the interaction of different variants of MBP with Zn^{2+} quantitatively using isothermal titration calorimetry (ITC). Figure 3 presents results from a typical ITC experiment, which was performed in triplicate for each recombinant murine MBP variant (Wiseman et al. 1989;

Velazquez-Campoy et al. 2004). The parameters derived are summarized in Table 1. The dissociation constants for all MBP variants appeared to be in a low micromolar range, specifically 15.4 μM ± 12% for rmC1 (Fig. 3a), 22.3 μM ± 14% for rmC8 (Fig. 3c), 41.8 μM ± 6.7% for UT-rmC1 (Fig. 3b), and 41.6 μM ± 10% for UT-rmC8 (Fig. 3d). The major differences between the tagged and untagged versions of MBP were observed at higher Zn^{2+}:MBP ratios. At that region of the curve, the data points deviated slightly from the mathematical fit in the case of the rmC1 and rmC8 variants, but this effect disappeared with the untagged proteins. In fact, for two MBP variants containing the hexahistidine tag, rmC1 and rmC8, the better mathematical fit was obtained using "two sets of sites model" (data not shown). After employing that model, the parameters of one set of binding sites appeared to be very similar to those generated by the "one set of sites" model, but the other set had higher dissociation constants (220 and 51 μM) with the values of n (number of ligands bound) equal to 5.1 and 4.7 for rmC1 and rmC8, respectively. This observation can be explained by less specific and physiologically irrelevant binding of Zn^{2+} to the His_6-tag of the proteins.

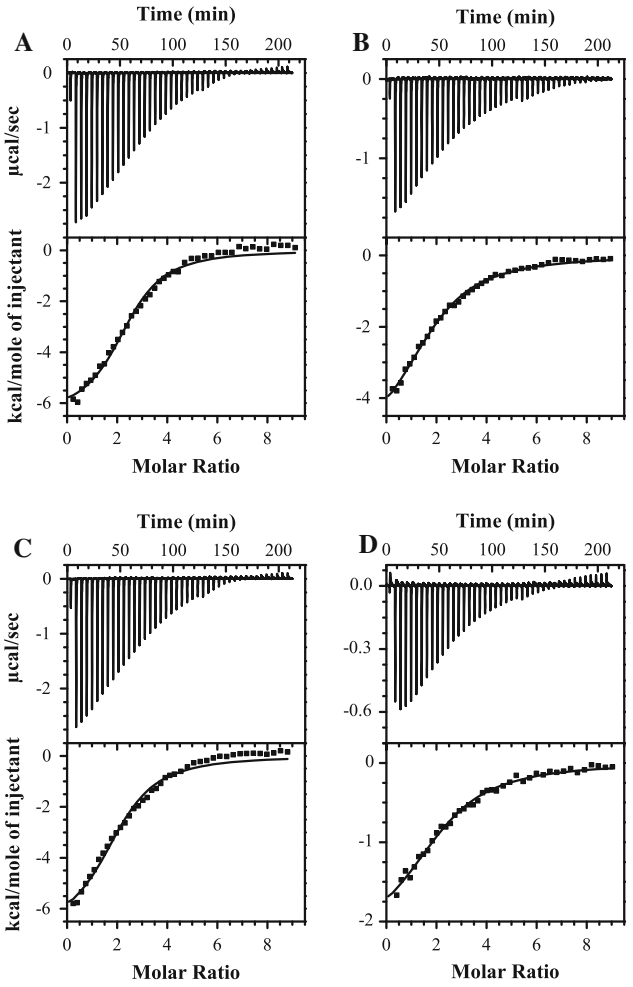

Fig. 3 Isothermal titration calorimetry (ITC) of Zn^{2+}-binding to rmMBP variants: **a** His_6-tagged rmC1, **b** UT-rmC1, **c** His_6-tagged rmC8, **d** UT-rmC8. A 50 μM protein solution (20 mM HEPES-NaOH, 100 mM NaCl, pH 7.4) was titrated with a 2.5 mM solution of $ZnCl_2$ at 25 °C. The data were fitted to the Origin "one set of sites" model. All parameters are summarized in Table 1

Effects of Zn^{2+} on rmMBP and UT-rmMBP in aqueous solution—CD spectroscopy

We next examined the characteristics of the UT-rmMBPs compared to His_6-tagged rmMBPs by using circular dichroism (CD), in aqueous solution in the absence of lipids. Previous CD spectroscopic experiments have shown that rmC1 and rmC8 in aqueous solution are primarily unstructured (Bates et al. 2000, 2002), and both UT-rmC1 and UT-rmC8 demonstrated similar characteristics, as anticipated (Fig. 4). After recording the CD spectra for UT-rmC1 and UT-rmC8 in the absence of divalent cation, we then added Zn^{2+} to a final concentration of 20 times molarity of the protein (1.3 mM). The Zn^{2+} induced only a slight increase in the large minimum and a slight decrease in the small minimum in both UT-rmC1 and UT-rmC8. It would be expected that solution NMR spectroscopy would reveal any local perturbations (Libich and Harauz 2008b), but here there were no detectable (by CD spectroscopy) global conformational changes of the protein interacting with the cation in aqueous solution.

Effects of Zn^{2+} on rmMBP and UT-rmMBP reconstituted with Cyt-LUVs—ATR-FTIR spectroscopy

It has long been known that detergents and lipids induce ordered secondary structure in MBP, particularly α-helix (e.g., Stuart 1996; Polverini et al. 1999); reviewed in (Harauz et al. 2004). However, reconstituting the recombinant MBP variants into a more myelin-mimetic environment, i.e., with Cyt-LUVs, yields semi-solid aggregates unsuitable for CD or, indeed, any type of solution spectroscopy (Libich and Harauz 2008b). Thus, ATR-FTIR spectroscopy (Haris and Chapman 1995; Barth 2007) was used next to examine the secondary structure composition of the four protein preparations in a lipid environment in the presence and absence of Zn^{2+}.

In our analyses, the ATR-FTIR spectra of all four rmMBP and UT-rmMBP variants in D_2O solution were normalized based on the amide I′ (deuterated amide I) absorbance. Since it has been reported that Zn^{2+} ions interact with the phospholipid headgroups (Nuzzo et al. 2002), we first present the spectra of a control experiment,

Table 1 Summary of ITC parameters

Recombinant MBP variant	K_a (M^{-1})	ΔH (kcal mol^{-1})	ΔS (cal mol^{-1} K^{-1})	n
rmC1	$(6.5 \pm 0.8) \times 10^4$	-6.50 ± 0.19	0.2	2.5 ± 0.1
rmC8	$(4.5 \pm 0.6) \times 10^4$	-6.92 ± 0.31	-1.9	2.1 ± 0.1
UT-rmC1	$(2.4 \pm 0.2) \times 10^4$	-5.69 ± 0.20	0.9	1.9 ± 0.1
UT-rmC8	$(2.4 \pm 0.2) \times 10^4$	-2.31 ± 0.31	12.28	2.3 ± 0.1

All measurements were carried out in triplicate at 25°C. The shown data represent the fitting parameters obtained using the "one set of sites" model. For each variant, "K_a" is the association constant, "ΔH" is change in enthalpy, "ΔS" is the change in entropy, and "n" is the number of ligands bound

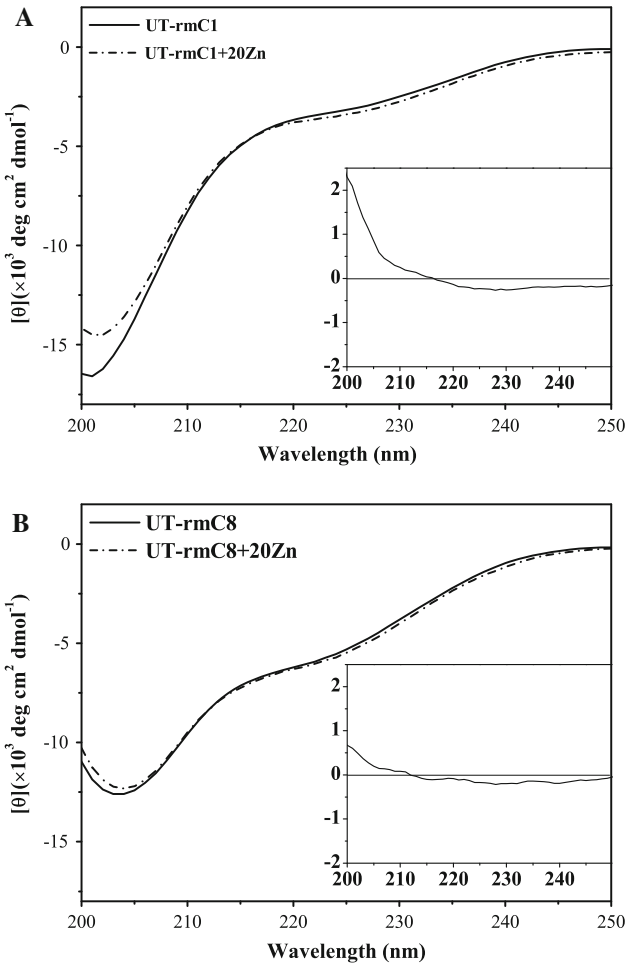

Fig. 4 CD spectroscopy of **a** UT-rmC1 and **b** UT-rmC8 in the absence (*solid line*) and presence (*dashed line*) of Zn^{2+}. The protein concentration was 1.3 mg mL^{-1} in a buffer containing 20 mM HEPES-NaOH, pH 7.4, 100 mM NaCl. Upon the addition of Zn^{2+}, the divalent cation was present at 1.3 mM concentration, or 20 times the molarity of protein. All spectra were collected at 25°C. Each CD spectrum shown in this figure is the average of three separate spectra. *Insets* in the bottom right corner of each plot depict the change in the averaged CD spectrum upon addition of Zn^{2+}

the Cyt-LUV lipid system (Fig. 5)—it is apparent that the membrane alone makes no significant contribution to the amide I′ region in the ATR-FTIR spectra.

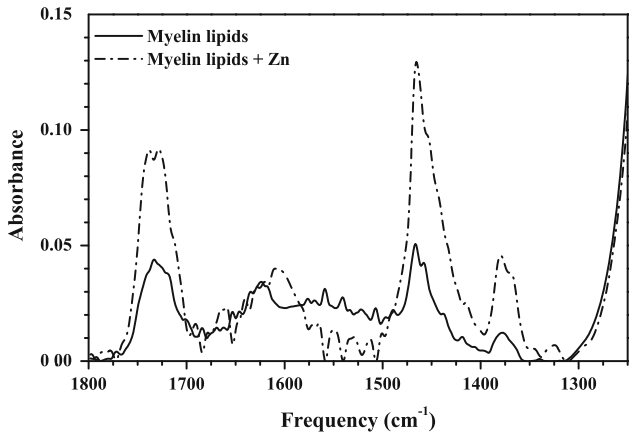

Fig. 5 ATR-FTIR spectroscopy of Cyt-LUVs alone in the absence (*solid line*) and presence (*dashed line*) of 4.1 mM Zn^{2+}. Note that there were no major changes observed in the amide I region (1,620–1,700 cm^{-1})

In Fig. 6, we present the ATR-FTIR spectra of rmC1, rmC8, UT-rmC1, and UT-rmC8 protein variants associated with Cyt-LUVs, in the absence and presence of Zn^{2+} at a 20-fold molar excess (4.1 mM). In Fig. 7, we present summaries of the ordered secondary structure predictions for all samples, derived from analyses of multiple spectra within the range 1,680 and 1,620 cm^{-1} corresponding to the amide I band (Byler and Susi 1986; Barth 2007). It should be cautioned that the calculations of overall secondary structure composition from such spectra might vary depending on the type of peak identification and fitting performed (Barth 2007; Goormaghtigh et al. 2009; Laird et al. 2009). Thus, comparisons with previous FTIR spectroscopic studies on natural MBP preparations in different reconstituted lipid systems (Surewicz et al. 1987; Nabet et al. 1994; Stuart 1996) would be confusing, so we restrict ourselves here simply to reporting on trends.

First, all spectra are characterized by a maximum around 1,639 cm^{-1}, and all show reproducible perturbations upon the addition of cation. Second, the addition of Zn^{2+} does not alter the degree of ordered secondary structure (α-helix, parallel and anti-parallel β-sheet, or β-turn) of any protein sample dramatically, but there are subtle variations. For

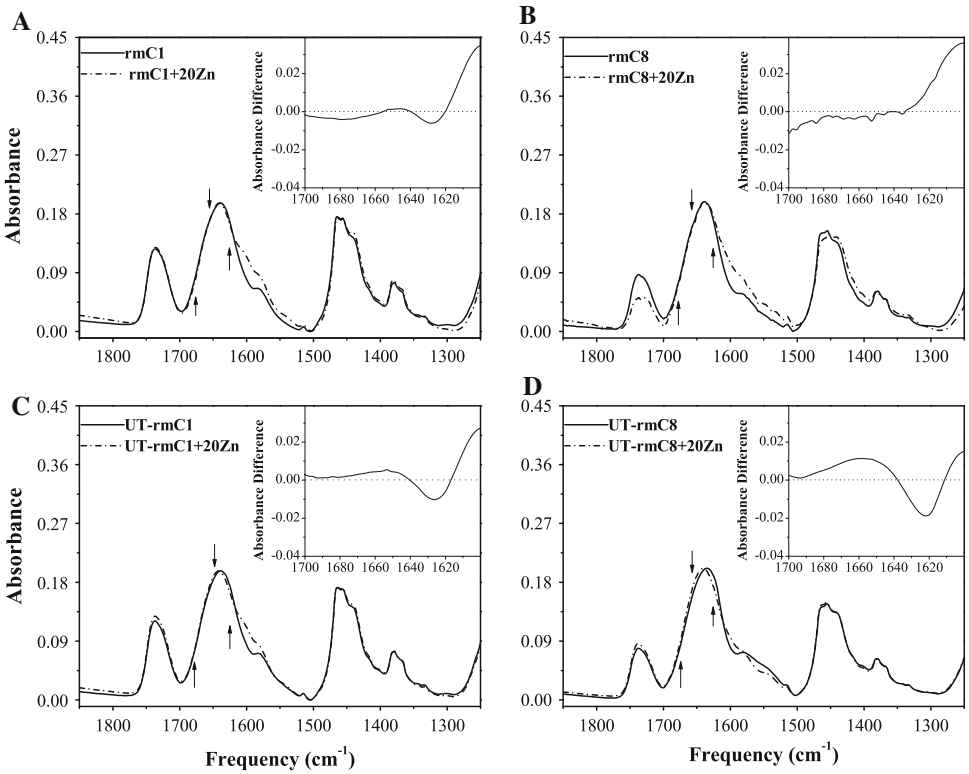

Fig. 6 ATR-FTIR spectroscopy of membrane-reconstituted **a** His_6-tagged rmC1, **b** His_6-tagged rmC8, **c** UT-rmC1, **d** UT-rmC8 in the absence (*solid line*) and presence (*dashed line*) of 4.1 mM Zn^{2+}. Protein samples and large unilamellar vesicles (LUV) were prepared in 20 mM HEPES-NaOH, pH 7.4, 100 mM NaCl at concentration of 4 mg mL^{-1}. We mixed 1 mg protein with lipid at 1:1 mass ratio (for details see "Materials and Methods"), *Arrows* at 1,657 cm^{-1} denote the presence of α-helix, and those at 1,629 cm^{-1}, and 1,675 cm^{-1} denote the presence of *β*-sheet structures. *Insets in the upper right* show the difference between spectra collected before and after the addition of Zn^{2+}

either rmC1 or rmC8, the changes are negligible except perhaps for rmC8, which appears to have a slight increase (a few percent) in amount of α-helix with a concomitant decrease in amount of *β*-turn. These same trends were observed more clearly for the untagged variants, both UT-rmC1 and UT-rmC8. These findings suggest that, in a lipid environment, UT-rmC1 and UT-rmC8 are more susceptible than rmC1 or rmC8, respectively, to secondary structural changes induced by Zn^{2+}-binding. Removal of the hexahistidine tag from the rmC1 and rmC8 variants is thus important to examine the proteins' ability to interact with metal ions in a lipid environment, and justifies the construction of the UT-rmC1 and UT-rmC8 variants. Although the conformational transitions induced by Zn^{2+}-binding are subtle, they are of a nature consistent with the idea of zinc being a stabilizing component of myelin.

Zinc-induced secondary structure transitions in membrane-associated MBP

Structural studies of IDPs such as MBP must take into account the sensitivity of the protein's conformation to exposure to different environments (Harauz et al. 2004, 2009; Zhong et al. 2007; Libich and Harauz 2008b; Harauz and Libich 2009; Libich et al. 2010; Uversky 2009). Here, partly in this context, we have tested specifically the hypothesis that Zn^{2+} induces ordered secondary structure in 18.5 kDa MBP. Divalent cations such as Zn^{2+} have been shown to lead to a disorder-to-order transition in several other IDPs (Gatewood et al. 1990; Uversky et al. 2000; Uversky 2009), but this is not necessarily the case for all IDPs (Uversky et al. 2002; Permyakov et al. 2002). The 18.5 kDa MBP has long been known to have a strong association with copper (Moscarello et al. 1968), and subsequent studies have reported that the protein binds divalent cations, $Hg^{2+} > Cu^{2+} > Zn^{2+} > Mg^{2+} > Cd^{2+} > Co^{2+}$ in decreasing order of affinity (Berlet et al. 1994). We focused here on zinc for physiological relevance, as discussed in the "Introduction".

It is seen in Fig. 7 that removal of the hexahistidine tag resulted in a subtly different pattern of conformational changes of the recombinant proteins when complexed with an excess of Zn^{2+} in a myelin-mimetic lipid environment, particularly a small increase in α-helix and concomitant decrease in *β*-turn content. One explanation may be as follows. Deuterated arginine side chains absorb at wavenumbers of 1,607 and 1,583 cm^{-1}. At both of these frequencies, there are significant absorbance increases upon the addition of Zn^{2+} in all four rmMBP constructs studied here (rmC1, rmC8, UT-rmC1, and UT-rmC8). This observation suggests that zinc may compete with the arginine residues for interaction with the phospholipid headgroups, resulting in the "release" of these side chains from the membrane (cf., Cabiaux et al. 1994), and a concomitant conformational change. Moreover, the observation that Zn^{2+} added to any protein variant alone (i.e., in

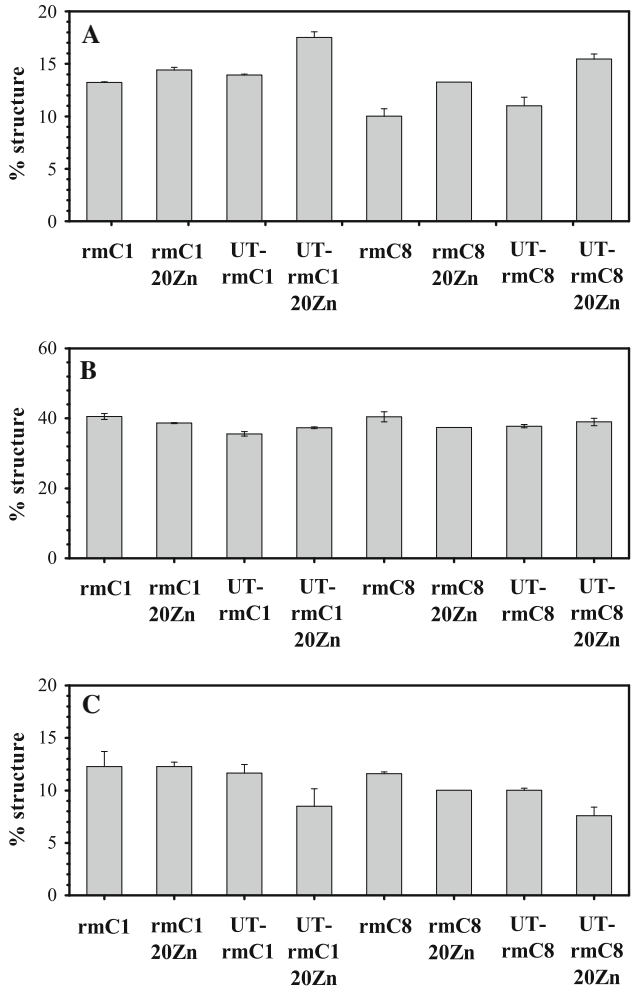

Fig. 7 Summary of ordered secondary structure assignments including **a** α-helix, **b** parallel and anti-parallel β-sheet, **c** β-turn. Each *bar* represents the average of two or more independent experiments (of different protein preparations and/or different reconstitutions), and the *error bars* represent the standard deviation

aqueous solution, Fig. 4) did not significantly alter the secondary structure composition confirmed that there is a synergy of MBP-membrane-cation interactions (Cavatorta et al. 1994; Riccio et al. 1995; Morante 2001; Nuzzo et al. 2002; Benfatto et al. 2004).

Two other recent biophysical studies support our conclusion of zinc-induced conformational changes in MBP. First, Majava et al. (2009) have independently shown changes in synchrotron CD spectra of natural porcine 18.5 kDa MBP dissolved in phosphate buffer, upon titration with Zn^{2+}. Their use of phosphate buffer (in contrast to our aqueous solution) may have yielded aggregates of protein, zinc, and phosphate (Cavatorta et al. 1994), thus representing a synergistic association that we mimicked in the solid-state. Secondly, Baran et al. (2010) have recently used nanopore analysis to demonstrate a cation-induced compaction of the same rmMBP variants studied here, suggestive of a higher-order topology such as the "paperclip" fold of tau (von Bergen et al. 2006; Jeganathan et al. 2006; Mukrasch et al. 2009). The conditions in this separate nanopore study required very high salt concentrations (1 M KCl), however, which made correlative secondary structure analysis by CD spectroscopy impossible. Conversely, nanopore analysis could not be performed on the semi-solid membrane-reconstituted protein samples that we have studied here. Nevertheless, the formation of a more compact tertiary fold in the presence of the cation may also account for some of the changes in secondary structure composition that we have observed here.

Conclusions

Two new recombinant forms of the classic 18.5 kDa MBP family, namely UT-rmC1 and UT-rmC8, were overexpressed and purified to greater that 96% purity via a native lysis procedure and ion-exchange chromatography, without the use of an appended purification tag. From 1 L of *E. coli* bacterial culture, 8 and 6 mg of UT-rmC1 and UT-rmC8 were isolated, respectively, and their secondary structures were probed in the absence and presence of Zn^{2+} using CD spectroscopy and ATR-FTIR spectroscopy. Circular dichroism revealed that there was little to no change in secondary structure in either protein variant alone upon the addition of Zn^{2+}. In contrast, using ATR-FTIR spectroscopy in a reconstituted membrane environment, Zn^{2+} caused a small but reproducible shift in overall ordered secondary structure of both UT-rmC1 and UT-rmC8, compared to their tagged counterparts. These studies suggest that divalent cations such as Zn^{2+} would have a stabilizing effect on MBP reconstituted within increasingly complex myelin-mimetic environments for solid-state NMR spectroscopic studies (Zhong et al. 2007; Ahmed et al. 2009; Libich et al. 2010).

Acknowledgments This work was supported by the Canadian Institutes of Health Research (MOP #74468, to G.H. and Vladimir Ladizhansky), the Natural Sciences and Engineering Research Council of Canada (G.H.), and the Advanced Foods and Materials Network Centre of Excellence (G.H. and J.R.D.). G.S.T.S. and V.V.B. are the recipients of a Doctoral Studentship and a Postdoctoral Fellowship, respectively, from the Multiple Sclerosis Society of Canada. G.S.T.S. was initially the recipient of a stipend from an anonymous private donor in support of this work. J.R.D. acknowledges support from the Canada Research Chair Program. The authors are grateful to Drs. Mumdooh Ahmed, Vladimir Ladizhansky, and Leonid Brown (Physics, University of Guelph) for their advice on ATR-FTIR data collection and analysis, and to Dr. Joan Boggs (Hospital for Sick Children, Toronto) and Dr. Jeremy Lee (University of Saskatoon) for comments on the manuscript.

References

Ahmed MA, Bamm VV, Shi L, Steiner-Mosonyi M, Dawson JF, Brown L, Harauz G, Ladizhansky V (2009) Induced secondary structure and polymorphism in an intrinsically disordered structural linker of the CNS: solid-state NMR and FTIR spectroscopy of myelin basic protein bound to actin. Biophys J 96:180–191

Bailey RW, Dunker AK, Brown CJ, Garner EC, Griswold MD (2001) Clusterin, a binding protein with a molten globule-like region. Biochemistry 40:11828–11840

Bamm VV, Harauz G (2008) Expression and purification of the active variant of recombinant murine Golli-interacting protein (GIP)—characterization of its phosphatase activity and interaction with Golli-BG21. Protein Expr Purif 62:36–43

Baran C, Smith GS, Bamm VV, Harauz G, Lee JS (2010) Divalent cations induce a compaction of intrinsically disordered myelin basic protein. Biochem Biophys Res Commun 391:224–229

Barth A (2007) Infrared spectroscopy of proteins. Biochim Biophys Acta 1767:1073–1101

Bartlett G (1959) Phosphorus assay in column chromatography. J Biol Chem 234:466–468

Bates IR, Matharu P, Ishiyama N, Rochon D, Wood DD, Polverini E, Moscarello MA, Viner NJ, Harauz G (2000) Characterization of a recombinant murine 18.5-kDa myelin basic protein. Protein Expr Purif 20:285–299

Bates IR, Libich DS, Wood DD, Moscarello MA, Harauz G (2002) An Arg/Lys– > Gln mutant of recombinant murine myelin basic protein as a mimic of the deiminated form implicated in multiple sclerosis. Protein Expr Purif 25:330–341

Benfatto M, Della LS, Qin Y, Li Q, Pan G, Wu Z, Morante S (2004) The role of Zn in the interplay among Langmuir–Blodgett multilayer and myelin basic protein: a quantitative analysis of XANES spectra. Biophys Chem 110:191–201

Berlet HH, Ilzenhofer H, Gass P (1991) Restricted endogenous proteolysis of myelin basic protein of zinc-treated myelin. Acta Neurol (Napoli) 13:145–152

Berlet HH, Bischoff H, Weinhardt F (1994) Divalent metals of myelin and their differential binding by myelin basic protein of bovine central nervous system. Neurosci Lett 179:75–78

Boggs JM (2006) Myelin basic protein: a multifunctional protein. Cell Mol Life Sci 63:1945–1961

Boggs JM (2008) Myelin basic protein. Nova Science Publishers, Hauppauge

Boggs JM, Yip PM, Rangaraj G, Jo E (1997) Effect of posttranslational modifications to myelin basic protein on its ability to aggregate acidic lipid vesicles. Biochemistry 36:5065–5071

Byler DM, Susi H (1986) Examination of the secondary structure of proteins by deconvolved FTIR spectra. Biopolymers 25:469–487

Cabiaux V, Agerberth B, Johansson J, Homble F, Goormaghtigh E, Ruysschaert JM (1994) Secondary structure and membrane interaction of PR-39, a Pro + Arg-rich antibacterial peptide. Eur J Biochem 224:1019–1027

Carré JL, Goetz BD, O'Connor LT, Bremer Q, Duncan ID (2002) Mutations in the rat myelin basic protein gene are associated with specific alterations in other myelin gene expression. Neurosci Lett 330:17–20

Cavatorta P, Giovanelli S, Bobba A, Riccio P, Szabo AG, Quagliariello E (1994) Myelin basic protein interaction with zinc and phosphate: fluorescence studies on the water-soluble form of the protein. Biophys J 66:1174–1179

Earl C, Chantry A, Mohammad N, Glynn P (1988) Zinc ions stabilise the association of basic protein with brain myelin membranes. J Neurochem 51:718–724

Gatewood JM, Schroth GP, Schmid CW, Bradbury EM (1990) Zinc-induced secondary structure transitions in human sperm protamines. J Biol Chem 265:20667–20672

Goormaghtigh E, Gasper R, Benard A, Goldsztein A, Raussens V (2009) Protein secondary structure content in solution, films and tissues: redundancy and complementarity of the information content in circular dichroism, transmission and ATR FTIR spectra. Biochim Biophys Acta 1794:1332–1343

Harauz G, Libich DS (2009) The classic basic protein of myelin—conserved structural motifs and the dynamic molecular barcode involved in membrane adhesion and protein–protein interactions. Curr Protein Peptide Sci 10:196–215

Harauz G, Ishiyama N, Hill CMD, Bates IR, Libich DS, Farès C (2004) Myelin basic protein—diverse conformational states of an intrinsically unstructured protein and its roles in myelin assembly and multiple sclerosis. Micron 35:503–542

Harauz G, Ladizhansky V, Boggs JM (2009) Structural polymorphism and multifunctionality of myelin basic protein. Biochemistry 48:8094–8104

Haris PI, Chapman D (1995) The conformational analysis of peptides using Fourier transform IR spectroscopy. Biopolymers 37:251–263

Hill CMD, Haines JD, Antler CE, Bates IR, Libich DS, Harauz G (2003) Terminal deletion mutants of myelin basic protein: new insights into self-association and phospholipid interactions. Micron 34:25–37

Ho SY, Catalanotto FA, Lisak RP, Dore-Duffy P (1986) Zinc in multiple sclerosis II: Correlation with disease activity and elevated plasma membrane-bound zinc in erythrocytes from patients with multiple sclerosis. Ann Neurol 20:712–715

Inouye H, Kirschner DA (1984) Effects of $ZnCl_2$ on membrane interactions in myelin of normal and shiverer mice. Biochim Biophys Acta 776:197–208

Inouye H, Kirschner DA (1988) Membrane interactions in nerve myelin: II. Determination of surface charge from biochemical data. Biophys J 53:247–260

Itoh M, Ebadi M, Swanson S (1983) The presence of zinc-binding proteins in brain. J Neurochem 41:823–829

Iyengar GV, Koomer WE, Bown HJM (1978) The elemental composition of human tissues and body fluids. Verlag-Chemie, New York

Jeganathan S, von Bergen M, Brutlach H, Steinhoff HJ, Mandelkow E (2006) Global hairpin folding of tau in solution. Biochemistry 45:2283–2293

Keen CL, Taubeneck MW, Daston GP, Rogers JM, Gershwin ME (1993) Primary and secondary zinc deficiency as factors underlying abnormal CNS development. Ann N Y Acad Sci 678:37–47

Kim JK, Mastronardi FG, Wood DD, Lubman DM, Zand R, Moscarello MA (2003) Multiple sclerosis: an important role for post-translational modifications of myelin basic protein in pathogenesis. Mol Cell Proteomics 2:453–462

Koh JY (2001) Zinc and disease of the brain. Mol Neurobiol 24:99–106

Laird DJ, Mulvihill MM, Lillig JA (2009) Membrane-induced peptide structural changes monitored by infrared and circular dichroism spectroscopy. Biophys Chem 145:72–78

Libich DS, Harauz G (2008a) Backbone dynamics of the 18.5 kDa isoform of myelin basic protein reveals transient α-helices and a calmodulin-binding site. Biophys J 94:4847–4866

Libich DS, Harauz G (2008b) Solution NMR and CD spectroscopy of an intrinsically disordered, peripheral membrane protein: evaluation of aqueous and membrane-mimetic solvent conditions for studying the conformational adaptability of the 18.5 kDa isoform of myelin basic protein (MBP). Eur Biophys J 37:1015–1029

Libich DS, Robertson VJ, Monette MM, Harauz G (2004) Backbone resonance assignments of the 18.5 kDa isoform of murine myelin basic protein (MBP). J Biomol NMR 29:545–546

Libich DS, Ahmed MAM, Zhong L, Bamm VV, Ladizhansky V, Harauz G (2010) Fuzzy complexes of myelin basic protein - NMR spectroscopic investigations of a polymorphic organizational linker of the central nervous system. Biochem Cell Biol (Special issue on Protein Folding: Principles and Diseases). doi: 10.1139/O09-123

Majava V, Petoukhov MV, Hayashi N, Pirila P, Svergun DI, Kursula P (2008) Interaction between the C-terminal region of human myelin basic protein and calmodulin: analysis of complex formation and solution structure. BMC Struct Biol 8:10

Majava V, Wang C, Myllykoski M, Kangas SM, Kang SU, Hayashi K, Baumgärtel P, Heape AM, Lubec G, Kursula P (2009) Structural analysis of the complex between calmodulin and full-length myelin basic protein, an intrinsically disordered molecule. Amino Acids. doi:10.1007/s00726-009-0364-2

Mittag T, Kay LE, Forman-Kay JD (2009) Protein dynamics and conformational disorder in molecular recognition. J Mol Recognit 23:105–116

Mo ZY, Zhu YZ, Zhu HL, Fan JB, Chen J, Liang Y (2009) Low micromolar zinc accelerates the fibrillization of human Tau via bridging Cys291 and Cys322. J Biol Chem 284:34648–34657

Morante S (2001) The zinc environment in Langmuir–Blodgett phospholipid multi-layers. J Synchrotron Radiat 8:975–977

Moscarello MA, Murdoch D, Wood DD (1968) The effect of metals on the binding of 131-I-labelled acid-soluble protein to myelin in vitro. Can J Biochem 46:235–240

Mukrasch MD, Bibow S, Korukottu J, Jeganathan S, Biernat J, Griesinger C, Mandelkow E, Zweckstetter M (2009) Structural polymorphism of 441-residue tau at single residue resolution. PLoS Biol 7:e34

Musse AA, Boggs JM, Harauz G (2006) Deimination of membrane-bound myelin basic protein in multiple sclerosis exposes an immunodominant epitope. Proc Natl Acad Sci USA 103:4422–4427

Nabet A, Boggs JM, Pezolet M (1994) Study by infrared spectroscopy of the interaction of bovine myelin basic protein with phosphatidic acid. Biochemistry 33:14792–14799

Nuzzo S, Meneghini C, Mobilioo S, Haas H, Riccio P, Fasano A, Cavatorta P, Morante S (2002) An x-ray absorption spectroscopy study of the zinc environment in Langmuir-Blodgett phospholipid multilayers. Biophys J 83:3507–3512

Permyakov SE, Oberg KA, Cherskaya AM, Shavlovsky MM, Permyakov EA, Uversky VN (2002) Human alpha-fetoprotein as a Zn(2 +)-binding protein. Tight cation binding is not accompanied by global changes in protein structure and stability. Biochim Biophys Acta 1586:1–10

Polverini E, Fasano A, Zito F, Riccio P, Cavatorta P (1999) Conformation of bovine myelin basic protein purified with bound lipids. Eur Biophys J 28:351–355

Readhead C, Hood L (1990) The dysmyelinating mouse mutations shiverer (shi) and myelin deficient (shimld). Behav Genet 20:213–234

Riccio P, Giovannelli S, Bobba A, Romito E, Fasano A, Bleve-Zacheo T, Favilla R, Quagliariello E, Cavatorta P (1995) Specificity of zinc binding to myelin basic protein. Neurochem Res 20:1107–1113

Saeidian S, Saboury AA, Sanati H, Moosavi-Movahedi AA (2001) Thermodynamics of binding zinc ion on myelin basic protein (Meeting Poster Abstract). Biophys J 79(Supplement)

Sandstead HH, Frederickson CJ, Penland JG (2000) History of zinc as related to brain function. J Nutr 130:496S–502S

Stuart BH (1996) A Fourier transform infrared spectroscopic study of the secondary structure of myelin basic protein in reconstituted myelin. Biochem Mol Biol Int 38:839–845

Surewicz WK, Moscarello MA, Mantsch HH (1987) Fourier transform infrared spectroscopic investigation of the interaction between myelin basic protein and dimyristoylphosphatidylglycerol bilayers. Biochemistry 26:3881–3886

Susi H, Timasheff SN, Stevens L (1967) Infrared spectra and protein conformations in aqueous solutions. I. The amide I band in H2O and D2O solutions. J Biol Chem 242:5460–5466

Takeda A (2001) Zinc homeostasis and functions of zinc in the brain. Biometals 14:343–351

Tompa P, Fuxreiter M (2008) Fuzzy complexes: polymorphism and structural disorder in protein–protein interactions. Trends Biochem Sci 33:2–8

Tsang D, Tsang YS, Ho WK, Wong RN (1997) Myelin basic protein is a zinc-binding protein in brain: possible role in myelin compaction. Neurochem Res 22:811–819

Unal B, Tan H, Orbak Z, Kiki I, Bilici M, Bilici N, Aslan H, Kaplan S (2005) Morphological alterations produced by zinc deficiency in rat sciatic nerve: a histological, electron microscopic, and stereological study. Brain Res 1048:228–234

Uversky VN (2009) Intrinsically disordered proteins and their environment: effects of strong denaturants, temperature, pH, counter ions, membranes, binding partners, osmolytes, and macromolecular crowding. Protein J 28:305–325

Uversky VN, Gillespie JR, Millett IS, Khodyakova AV, Vasilenko RN, Vasiliev AM, Rodionov IL, Kozlovskaya GD, Dolgikh DA, Fink AL, Doniach S, Permyakov EA, Abramov VM (2000) Zn(2+)-mediated structure formation and compaction of the "natively unfolded" human prothymosin alpha. Biochem Biophys Res Commun 267:663–668

Uversky VN, Permyakov SE, Zagranichny VE, Rodionov IL, Fink AL, Cherskaya AM, Wasserman LA, Permyakov EA (2002) Effect of zinc and temperature on the conformation of the gamma subunit of retinal phosphodiesterase: a natively unfolded protein. J Proteome Res 1:149–159

Velazquez-Campoy A, Leavitt SA, Freire E (2004) Characterization of protein-protein interactions by isothermal titration calorimetry. Methods Mol Biol 261:35–54

von Bergen M, Barghorn S, Jeganathan S, Mandelkow EM, Mandelkow E (2006) Spectroscopic approaches to the conformation of tau protein in solution and in paired helical filaments. Neurodegener Dis 3:197–206

Wiseman T, Williston S, Brandts JF, Lin LN (1989) Rapid measurement of binding constants and heats of binding using a new titration calorimeter. Anal Biochem 179:131–137

Zhong L, Bamm VV, Ahmed MA, Harauz G, Ladizhansky V (2007) Solid-state NMR spectroscopy of 18.5 kDa myelin basic protein reconstituted with lipid vesicles: spectroscopic characterisation and spectral assignments of solvent-exposed protein fragments. Biochim Biophys Acta (Biomembranes) 1768:3193–3205